Caballero-Mancebo, E.; Moreno Rodríguez, JM.; Corma Canós, A.; Díaz Morales, UM.; Cohen, B.; Douhal, A. (2021). Deciphering the photobehaviour of ensemble and single crystals of Zr-based ITQ MOF composites. Journal of Photochemistry and Photobiology A Chemistry. 404:1-9. https://doi.org/10.1016/j.jphotochem.2020.112887

Contents lists available at ScienceDirect

Journal of Photochemistry & Photobiology, A: Chemistry

journal homepage: http://ees.elsevier.com

Deciphering the photobehaviour of ensemble and single crystals of Zr-based ITQ MOF composites

Elena Caballero-Mancebo [a], José María Moreno [b], Avelino Corma [b], Urbano Díaz [b,*], Boiko Cohen [a,*], Abderrazzak Douhal [a,*]

[a] Departamento de Química Física, Facultad de Ciencias Ambientales y Bioquímica, and INAMOL, Universidad de Castilla-La Mancha, Avenida Carlos III, S/N, 45071 Toledo, Spain
[b] Instituto de Tecnología Química, Universitat Politecnica de Valéncia-Consejo Superior de Investigaciones Científicas (UPV-CSIC), Av. de los Naranjos s/n, 46022 Valencia, Spain

ARTICLE INFO

Keywords
2D-MOF
Photodynamics
Energy transfer
Metal Cluster Effect
Composites

ABSTRACT

Understanding the interactions that govern the photophysical behaviour of Metal-organic frameworks (MOFs) and their composites is paramount for their photochemical and photonic applications. In this work, we report on the photobehaviour of Nile Red (NR) adsorbed on the surface of 2D Zr-ITQ-HB (NR@Zr-ITQ-HB) MOF using ultrafast (fs-ns) and single-molecule fluorescence techniques. The results show the occurrence of energy transfer processes happening in 0.34 ns between neighbouring NR molecules, intramolecular charge transfer reaction (~ 0.6 ps) and a vibrational cooling (10 ps) of the adsorbed dye. Time-resolved single-composite fluorescence microscopy experiments on different NR-loaded composites allowed to resolve the emission from adsorbed aggregates (0.9 ns) and from the charge separated state (2.5 ns) of excited NR. The different photobehaviour of NR adsorbed on ZrO_2 nanoparticles indicates the relevance of the Zr-ITQ-HB MOF´s surface to the observed photoinduced reactions in the composites. We discuss how the nature of both, the organic linkers and metal clusters in this kind of MOFs, affects the photodynamics of the composites. These results may help in designing MOFs "on demand" for their application in photons-based science and technology, like photocatalysis and lighting.

1. Introduction

Metal-organic frameworks (MOFs) are hybrid materials whose relevance for the scientific community has been established thanks to their wide range of properties and applications, covering so different fields of science and technology such as gas storage, optoelectronic devices and homeland security to cite few applications [1–5]. Even though the interest has been increasing, developing different structures with better properties, especially increasing their chemical stability, is still a challenge [6–8]. Working in this direction, it has been reported that MOFs formed by the same organic linkers present higher stability when the metal centres are composed by high-valent metal cations [8–12]. Thus, clusters of transition metals with high oxidation order may help in the improvement of this desirable property. Specifically, Zr-based MOFs have shown high chemical and thermal stability, mainly produced by the high affinity of Zr-cluster to oxygen ligands [11–13]. Furthermore, Zr-MOFs present several additional advantages, such as structural versatility or high charge density, which favor the interactions with organic molecules that can be hosted in or on their framework [4,8,12,14]. Recently, a new class of 2D-MOFs has been developed [15]. The morphology of these materials presents advantages over the 3D-MOFs, that might be beneficial for catalysis purposes. For example, the diffusion of guest molecules becomes easier through the lamellar structures than through the internal pores of the 3D-materials. In addition, the lack of connection between the sheets implies presence of free coordinated sites in the metal clusters that can act as active sites for the catalytic activity [15].

Recently, we have reported on studies of a 2D-MOFs based on Al clusters (Al-ITQ-HB) [16–18] and their composites when adsorbing Nile Red (NR) molecules. [19–21] This MOF, which presents high photocatalytic activity in water [22], shows promising properties as chemical support, favouring the interactions between neighbouring organic molecules located on its surface, giving rise to long-photoinduced energy transfer (ET) processes (0.3 – 2 ns). We have shown also that the ET event in the composites is affected by the nature of the MOF surface, being faster when the alkyl chain of the organic spacer is shorter (2 carbons vs 7 carbons) [20]. Furthermore, substituting the alkyl chain by an amino group (NH_2) inhibits the ET reaction due to the presence of electron transfer from the amino linker to the organic guest [20]. The possibility of tuning the interactions with the hosted molecules pushes forward the need to further explore the characteristics and related processes of this material, such as, for example, the effect of

* Corresponding authors.
E-mail addresses: udiaz@itq.upv.es (U. Díaz); Boyko.Koen@uclm.es (B. Cohen); Abderrazzak.Douhal@uclm.es (A. Douhal)

https://doi.org/10.1016/j.jphotochem.2020.112887
Received 12 May 2020; Received in revised form 7 August 2020; Accepted 1 September 2020
Available online xxx
1010-6030/

the metal cluster nature on the photobehaviours of the composite. Thus, it is of great interest to explore the advantages of Zr-based 2D-MOFs over 3D-MOFs with other metal clusters, by modification of the former 2D- M-ITQ-HB materials upon replacing the Al-based clusters by the Zr-ones, forming the Zr-ITQ-HB material [23]. Of relevance to the application of this new MOF in photonics and photocatalysis is the understanding of the photoinduced properties of the composites when interacting with organic molecules.

Here in, we report on a combination of steady-state observation, ultrafast dynamics and single-crystal fluorescence microscopy studies of NR molecules adsorbed on the surface of a 2D Zr-based MOF (NR@Zr-ITQ-HB). The steady-state experiment shows a broad absorption band, reflecting the presence of several absorbing NR species, while the narrow emission band indicates a common deactivation pathway to the ground state. Time-resolved observation reveals the presence of an ET event between neighbouring NR molecules (0.34 ns). The value of this time component is related with the polarity of the environment in the Zr-based composites. Femtosecond (fs) time-resolved experiments show that the adsorbed NR molecules exhibit an ultrafast intramolecular charge transfer (ICT) reaction in NR in ~ 0.6 ps, and a ~10 ps dynamics, assigned to vibrational cooling (VC) of NR molecules adsorbed on the MOF surface. Picosecond time-resolved fluorescence confocal microscopy experiments using composites having different NR loadings gave the emission of adsorbed NR aggregates (0.9 ns) and of the charge-separated (CS) state (~2.5 ns). NR supported on the surface of ZrO_2 NPs presents a strong emission quenching, probably due to an electron injection (EI) from the dye to the metal atoms. Our findings reported here may help in the design of new 2D MOFs for photonic and photocatalytic applications, and for a better understanding of the related photochemical reaction or photophysical processes.

2. Materials and methods

2.1. Structural characterization of Zr-ITQ-HB

Zr-ITQ-HB XRD analysis was performed with a Philips X'PERT diffractometer equipped with a detector and a secondary graphite monochromator. Data were collected stepwise over the $2^o \leq 2\theta \leq 20^o$ angular region, with steps of 0.02^o 2θ, 20 s/step accumulation time and CuKα (λ = 1.54178 Å) radiation. Transmission electron microscopy (TEM) micrographs were acquired with a JEOL JEM2100 F electron microscope operating at 200 keV. The samples were treated through the dispersion of the powders onto carbon copper grids. C, N and H contents were estimated with a Carlo Erba 1106 elemental analyzer, while the metal contents were determined through atomic absorption spectroscopy (Spectra AA 10 Plus, Varian).

2.2. Synthesis of NR@Zr-ITQ-HB composites

Nile Red (NR, Sigma-Aldrich, >98.0%) was adsorbed on the surface of the 2D-materials using a procedure already published [21]. For the synthesis of the NR/ZrO_2 composites, ZrO_2 (Sigma-Aldrich, particle size <50 nm) nanoparticles (NPs) were used. We followed the same procedure as for the MOF composites, by adding 50 mg of the NPs to 1 mL of the dye solution. The mixture was stirred, and the solvent was evaporated.

2.3. Spectroscopic and dynamic studies

The steady-state UV-visible absorption and fluorescence experiments were carried out using JASCO V-670 and FluoroMax-4 (Jobin-Yvone) spectrophotometers, respectively. The JASCO V-670 spectrophotometer is equipped with 60 mm integrating sphere ISN-723 allowing the studies in solid state (diffuse reflectance spectra). For these measurements, the Kubelka-Munk remittance function is used: $F(R) = (1 - R)^2/2R$, where R is the diffuse reflectance intensity from the sample. The picosecond (ps) time-resolved emission experiments have been performed employing a ps time-correlated single-photon counting (TSCPC) system. The samples were excited by 40 ps-pulsed (~1 mW, 40 MHz repetition rate) diode-lasers (PicoQuant) centred at 470 nm, with an instrument response function (IRF) of the apparatus of ~70 ps. Details on the experimental setup and analysis are described elsewhere [29]. The decays were deconvoluted and fitted to a multiexponential function using the FLUOFIT package (PicoQuant), which allows single and global fits. The quality of the fits as well as the number of exponentials were carefully selected based on the reduced χ^2 values (which were always below <1.2) and the distributions of the residuals. The femtosecond (fs) time-resolved emission decays of the samples in solid state were collected using a fluorescence up-conversion technique in reflection mode [19]. The sample was excited at 470 nm by the second harmonic of Ti:Sapphire oscillator (MaiTai SpectroPhysics) output (940 nm). The IRF of the whole setup (measured as the reflected signal of the pump signal) was ~300 fs. To analyse the fs-transients, we convoluted a multiexponential function with the IRF to fit the experimental data. The errors for the calculated time components were smaller than 15% in all cases. The confocal microscopy measurements were performed on a MicroTime 200 confocal microscope (PicoQuant), details of which are described elsewhere [30,31]. The excitation was conducted with the same diode laser used in the TSCPC experiment. The emission signal was collected using a 520-nm long pass filter (Chroma). The emission spectra were collected through a Shamrock ST-303i (Andor Technology) imaging spectrograph and detected by an Andor Newton EM-CCD camera (Andor Technology). To analyze the data, we used SymPhoTime Analysis software (PicoQuant) and the quality of the fits are also based on the reduced χ^2 values (which were always below <1.2) and the distributions of the residuals. The samples were measured in the solid state, which was prepared by dispersing a small amount of the solid powder over the coverslip and introducing it into the sample holder.

3. Results and discussion

3.1. Synthesis and structural characterization of the Zr-ITQ-HB, NR@Zr-ITQ-HB and NR/ZrO_2 composites

Briefly, the Zr-ITQ-HB material was synthesized from equimolar quantities of $ZrCl_4$ (0.5 mmol) and 4-heptylbenzoic acid (0.5 mmol), which were dissolved in 4 mL DMF. The solution was introduced into a stainless-steel autoclave, heated at 120 °C for 24 hours under autogeneous pressure and static conditions. Once it was cooled to room temperature, the solution was filtered with distilled water. Then, the sample was activated in methanol for 24 hours in order to efficiently remove the remaining unreacted linker and solvent molecules. Finally, the material was isolated and dried under vacuum at room temperature. A mesoscopic phase of Zr-ITQ-HB was obtained when the monoalkylcarboxylate linker heptilbenzoic acid was used as structural spacer. The material showed a XRD pattern with one intense (100) band at low 2θ angles range at 24 Å and even a broad band at 12 Å corresponding to (200) diffraction order was possible to be identified (Figure S1A). The micrographs obtained by TEM are shown in Figure S1B, where low order regularity of the cavities of the mesoscopic phase is observed. Elemental CHNS analysis (Table S1) of the metal-organic material Zr-ITQ-HB estimates the organic content of the spacers included in the final solid. In comparison with Zr-ITQ-HB material, the organic contribution for the previously published Al-ITQ-HB is lower (~35% wt) due to minor incorporation of the organic spacer generating a mesoscopic material with low order structuration.[19-21] In the case of Zr-ITQ-HB, the higher organic content was associated with the major presence of organic spacers that promoted a mesoscopic material with higher homogeneity and order. Figures S1C and S1D (thermogravimet-

ric, TG and differential thermal analysis, DTA curves, respectively) show the weight loss for the corresponding organic content in the hybrid materials and determine their hydrothermal stability. For all the hybrid materials, two different weight losses were detected without taking account the hydration water and residual DMF molecules occluded in the materials (80-150 °C). The first weight loss was observed at 250-400 °C, being associated to the hydrocarbon tails from monocarboxylate organic spacers used in the mesoscopic materials. This weight loss was also assigned to $AlO_4(OH)_2$ or $ZrO_4(OH)_2$ builder units present in the 1D inorganic chains, being this oxygen contribution the main reason for obtaining the higher organic content from TGA related to CHNS analysis. The highest difference was observed for Al-ITQ-HB samples, comparing organic content from TGA and elemental analysis, indicating probably that aluminium nodes were coordinated to more elevated number of hydroxylated species than Zr-ITQ-HB. The final weight loss was clearly observed from 450 to 600 °C range corresponding to aromatic fragments from the organic spacers present in the final hybrid materials.

3.2. Steady-state observations of NR@Zr-ITQ-HB and NR/ZrO_2

To begin with, we consider the steady-state UV-visible absorption of the Zr-ITQ-HB material (Figure S2). It shows only a narrow band below 300 nm which will not interfere with the absorption spectrum of NR. The absorption and emission spectra of the NR@Zr-ITQ-HB composites in solid state are shown in Fig. 1A. Scheme I shows the chemical structure of NR and the Zr-ITQ-HB materials. The absorption spectrum exhibits a single band with maximum of intensity at 566 nm (Fig. 1A). The broadness of the band (Full Width at Half Maximum, FWHM, ~ 5970 cm^{-1}) suggests the presence of several co-existing species at S_0. In comparison with the spectrum of NR@Al-ITQ-HB composites (Figure S3), the absorption band of the former is broader. Here, we also observe a shoulder located at ~ 650 nm, which suggests the presence of additional NR conformations or aggregation states not present in Al-ITQ-HB. On the other hand, the NR@Zr-TIQ-HB emission spectrum is composed by a narrow band (FWHM ~ 1220 cm^{-1}) located at 688 nm. This spectrum has comparable shape to the NR@Al-ITQ-HB one, but is shifted by ~ 20 nm (~ 400 cm^{-1}) to longer wavelengths. This redder emission suggests either a higher aggregation tendency of NR molecules on the Zr-ITQ-HB surface. In similarity to the NR@Al-ITQ-HB composites, the emission spectra show some dependence on the excitation wavelength (Figure S4A), which indicates different origins of the emitters. The excitation spectra and the absorption one have the intensity maxima at the same wavelength, while the shape of the former is narrower, suggesting the involvement of non-radiative processes at S_1 of some of the NR species absorbing at the reddest tail of the absorption spectrum (Figure S4B).

To get more insight on the behaviour of NR molecules absorbed on the Zr-ITQ-HB surface, we studied NR adsorbed on the surface of ZrO_2 nanoparticles (NPs). Fig. 1A shows the related absorption spectrum. Both, the shape and location of the band, are very similar to the NR@Zr-ITQ-HB ones, which suggests that for the ZrO_2 NPs the environment and the dye distribution are comparable to those of the MOF giving rise to ground-state species that are similar in both composites. However, while the absorption spectra are comparable, we were not able to record an accurate emission spectrum of NR/ZrO_2, most probably due to the limited sensitivity of the equipment to detect a very low emission. This indicates that the absorbed NR molecules are undergoing a strong emission quenching. A previous report on the behaviour of NR/Al_2O_3 NPs revealed a similar absorption spectrum to the NR/ZrO_2 one [21]. Nevertheless, NR and alumina-based composites present a strong emission spectrum analogous to that of the NR interacting with the MOF. Thus, the ZrO_2 NPs affect the NR in a different way than the MOF or the Al_2O_3 NPs do. Time-resolved data will provide more information on the dynamics and keys of the related events in NR@Zr-ITQ-HB and NR/ZrO_2 composites.

3.3. Picosecond time-resolved fluorescence experiments

3.3.1. NR@Zr-ITQ-HB ps-time-resolved measurements

In order to determine how the nature of the metal cluster affects (Zr vs Al) the photodynamics of the adsorbed NR molecules, we carried

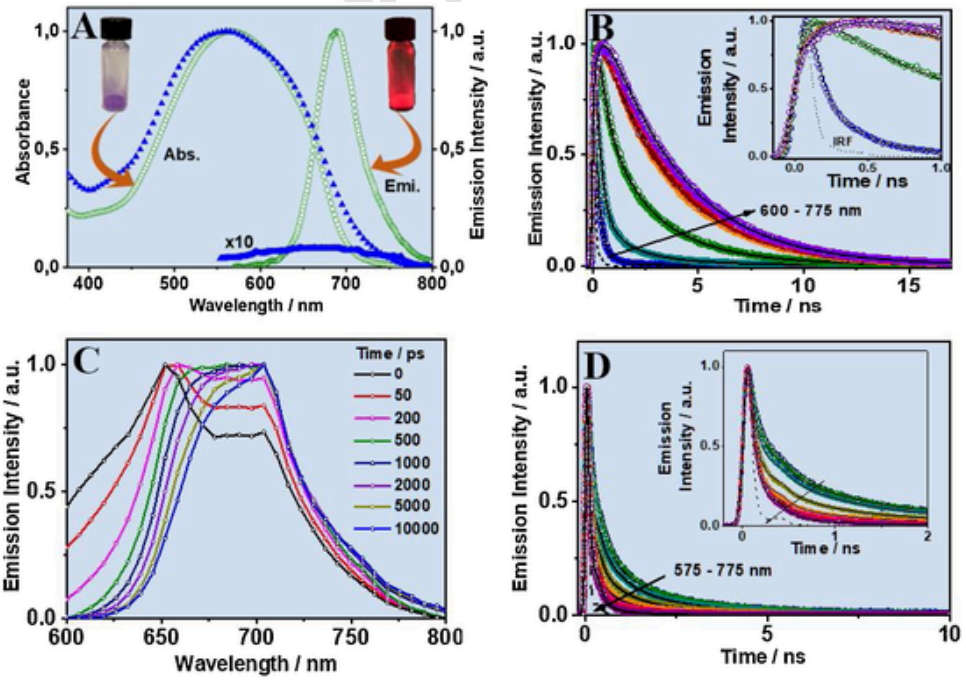

Fig. 1. (A) Steady-state UV-visible absorption and emission spectra of NR@Zr-ITQ-HB (green circles) and NR/ZrO_2 (blue triangles) in solid state (the emission spectrum intensity of NR/ZrO_2 sample was multiplied by 10). The inserts show an image of the sample and of the sample under the UV-lamp (360 nm). (B and C) Normalized magic-angle emission decays and Time-Resolved Emission Spectra of NR@Zr-ITQ-HB upon excitation at 470 nm. (D) Normalized magic-angle emission decays of NR/ZrO_2 upon excitation at 470 nm.

out ps time-resolved emission experiments on NR@Zr-ITQ-HB composites in solid state. Fig. 1B shows the recorded emission decays at different observation wavelengths upon excitation at 470 nm. Table 1 gives the values of the lifetimes, the pre-exponential factors and relative contributions (normalized to 100) obtained from accurate multiexponential fits of the recorded emission decays. We got four components of 0.15, 0.34, 1.18 and 3.31 ns. The shortest one (0.15 ns) has its highest contribution at the bluest part of the emission spectrum and decreases until it disappears at 675 nm. This component is assigned to the emission from the locally excited (LE) state of the NR molecules. This emission was previously characterized in NR@Al-ITQ-HB composites (~ 0.22 ns), having comparable emission behaviour [19,21]. The intermediate component (0.34 ns) decays at the blue side of the emission spectrum and becomes a rising one between 675 nm to 775 nm. We attribute this component to homo energy transfer (ET) process between neighbouring NR molecules adsorbed on the MOF surface. This time in the NR@Zr-ITQ-HB composites is slightly longer than the one observed in the NR@Al-ITQ-HB for the same concentration of NR at the 2D-MOF surface for the same photoevent (~ 0.22 ns) [21]. The difference is explained in terms of a change in the polarity of the environment due to the differences in the 2D-MOFs compositions. In addition to the metal clusters difference (Zr vs Al), the elemental C,H,N and S analysis (Table S1) of both metal-organic materials shows that the organic linkers contribution in Al-ITQ-HB is lower (~35% wt) than in the Zr-based material (~ 48% wt). This is due to a weaker incorporation of the organic spacer in the former. In the case of Zr-ITQ-HB, the larger organic content promotes the mesoscopic material with a higher homogeneity and ordered structure. The emission lifetime of 1.18 ns is attributed to a combination of those of NR aggregates and species having suffered an ICT reaction, while the longest one (~ 3.3 ns) is due to species as a result of ET reaction. For NR@Al-ITQ-HB, these two lifetimes were 1.33 and 3.61 ns, respectively. The changes in their values are within the experimental error, suggesting that the organic content in this case does not affect significantly the related relaxation pathways of the involved species.

In order to further elucidate the photobehaviour of the NR@Zr-ITQ-HB composites, we recorded the ps Time-Resolved Emission Spectra (TRES). Fig. 1C shows the normalized to the maximum of intensity TRES, and Figure S5 exhibits the not-normalized ones. At short times (< 200 ps) a band between 600 and 650 nm appears, and its intensity decreases until it disappears at ~ 1 ns delay. Thus, this band corresponds to the recorded shortest lifetime (0.15 ns) in the emission signal, and it is assigned to the LE state of adsorbed NR molecules. The TRES gated at shorter times present a second band at 650 nm, which losses its emission intensity while a second one located at 700 nm raises concomitantly. The time evolution of these bands corresponds to the ET process, resulting in the long emitting species (3.31 ns). To get more information on the spectral evolution, we deconvoluted the TRES collected at short (< 0.1 ps) and at long (10 ns) times. Fig. 2 and Table S2 show the spectral characteristics of the resulting bands. The < 0.1-ps spectrum reveals the presence of three emitting species having intensity maxima at ~ 625, ~ 650 and ~ 700 nm, and with contributions of 37, 11 and 52 %, respectively (Table 2). The 10-ns spectrum is completely shaped by a band located at ~700 nm, which is very similar to the band, located at 700 nm and observed at the early-time spectrum. Thus, both bands arise from the same emitters and correspond to the species resulting from the ET process. The band at ~ 650 nm that is present at short times is assigned to the emission from aggregates population. Similar tendency to aggregates formation for NR interacting with heterogenous supports, such as 3D- and 2D-MOFs, has been reported [19–21,24]. Finally, the band at ~ 625 nm that vanishes at times longer than 0.5 ns is assigned to the emission from the LE state. The analysis and deconvolution of the TRES allow us to distinguish the emissive species not observed in the steady-state spectrum, where we recoded a single band located at 688 nm. The steady-state spectrum is comparable to the one of the ET species emission (TRES collected at 10 ns), which suggests that the most efficient deactivation pathway of adsorbed NR molecules is the subsequent of the ET reaction. The small spectral position shift between both spectra sug-

Table 1
Values of the lifetimes, their pre-exponential factors (a_i) and contributions (c_i) normalized to 100 of NR@Zr-ITQ-HB upon excitation at 470 nm in solid state. The negative sing for a_i indicates a rising component in the emission signal.

$\lambda_{Obs/nm}$	τ_1/ns (±0.05)	a_1	c_1	τ_2/ns (±0.05)	a_2	c_2	τ_3/ns (±0.20)	a_3	c_3	τ_4/ns (±0.20)	a_4	c_4
600	0.15	87	54	0.34	11	32	1.18	-	-	3.31	2	14
625		60	21		27	20		7	18		6	41
650		3	1		34	7		37	34		26	58
675		-	-		-100	-100		40	22		60	78
700		-	-		-100	-100		35	15		65	85
725		-	-		-100	-100		12	7		88	93
750		-	-		-100	-100		-	-		100	100
775		-	-		-100	-100		-	-		100	100

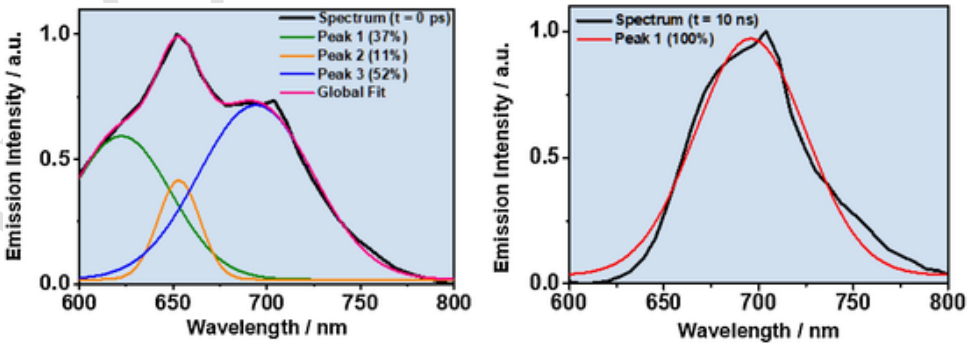

Fig. 2. Deconvoluted spectra of NR@Zr-ITQ-HB at different gating times: (A) 0 ps, and (B) 10 ns.

Table 2
Location, broadness (FWHM) and area of the resulting bands after the deconvolution of the emission spectra of NR@Zr-ITQ-HB at different gating times.

Gating time/ ns	Band 1			Band 2			Band 3		
	Max / nm	FWHM / nm	A	Max / nm	FWHM / nm	A	Max / nm	FWHM / nm	A
0	622	63	37	653	26	11	695	72	52
10	-			-			696	69	100

gests that although the most relevant photoinduced process is the ET reaction, we cannot neglect the presence of other processes that contribute to the total emission of the composites. The TRES of NR@Zr-ITQ-HB and NR@Al-ITQ-HB composites at both, short and long gating times, show interesting spectral and dynamical differences (Figure S6). At short times, the Al-based composite presents a single broad band with maximum of intensity at ~ 675 nm, while for the Zr-one even at the earliest times at least two different bands can be observed already. This suggests that the reddest band arises from species resulting from the ET event. This band is better separated from the one assigned to the LE in comparison with the NR@Al-ITQ-HB spectrum. We explain it in terms of a stronger interaction between NR molecules and the Zr-clusters, leading to NR species of lower energies favouring the intermolecular interactions.

3.3.2. NR/ZrO_2 ps-time-resolved measurements

The ps-time evolution of the NR/ZrO_2 NPs composites emission was recorded as a reference material. Fig. 1D shows the emission decays upon excitation at 470 nm, and the fitting data using triexponential functions are posted in Table S2. The emission decays for this composite reveal much faster deactivation processes than in NR@Zr-ITQ-HB. The observed components, of time constants of 0.13, 0.67 and 2.05 ns, decay along the whole emission spectrum. Previously, we showed that NR/Al_2O_3 NPs composites exhibit three emission lifetimes (0.17, 0.72 and 1.59 ns), which are like those of NR/ZrO_2 [21]. The two shortest components were assigned to aggregates emission, while the longest one to the emission of NR monomers. In the present composites, while the relative contribution of the two longer components (0.67 and 2.05 ns) decreases at longer wavelengths, the contribution of the shortest one increases. Although the time values are not very different, the spectral evolution is opposite to the one observed for the NR/Al_2O_3 NPs. This suggests presence of additional or different photoinduced processes that condition the NR photobehaviour when adsorbed on ZrO_2 NPs. Previous studies of NR interacting with Zr-doped mesoporous materials (MCM41) have reported on an electron injection (EI) from NR to trap states formed by the Zr d-orbitals that have lower energy than the ones of the excited dye [25,26]. This may explain the decrease in the lifetimes observed here in comparison with the NR@Zr-ITQ-HB ones and the different spectral evolution in comparison with the Al-based NPs. For the NR@Zr-ITQ-HB composites, due to the high concentration of the dye, most likely a multilayer distribution is achieved on the MOF surface. This, in combination with the low proportion of the inorganic part of this material (Table S1) results in an environment where the NR molecules are not directly affected by the Zr-clusters. This deactivates the processes associated with interaction with the Zr-ITQ-HB surface trap states. Moreover, contrary to the behaviour observed in NR@Zr-ITQ-HB, no rising component is observed in the emission decays of the NR/ZrO_2 composite. This indicates that the ET process is not present in this composite due to competition with other more efficient relaxation pathways. The large difference between the dynamics of NR when located on the Zr-ITQ-HB surface and on the ZrO_2 NPs establishes the relevance of the material properties to the adsorbed dye photobehaviour.

3.4. Femtosecond time-resolved fluorescence experiments

To decipher the photobehaviour of NR interacting with Zr-ITQ-HB material at a very short scale, we carried out femtosecond (fs) emission experiments on NR@Zr-ITQ-HB composites upon excitation at 470 nm in the solid state. Fig. 3A shows the obtained emission transients, and Table 3 gives the data from multiexponential fits. The transients are fitted using four components giving times of: ~ 0.60, ~ 10, ~ 150 and 300 ps, in addition to a ns-one fixed in the fit. In the previous paragraph, we already discussed the origin of the ns-fluorescence lifetime. The 300-ps component decays at the green region of the emission spectrum and rises at the red one (Fig. 3B), while the 150-ps one behaves as a decay along the whole emission spectrum. Both time constants have comparable values to those observed in the ps-experiments. Thus, we assign them to the emission of NR from its LE state, the ET process and aggregates emission, respectively (Scheme 1). The sub-ps component (0.6 ps), which decays at the shortest wavelengths of the emission spectrum, and rises at the longest one, is assigned to the ICT reaction of adsorbed NR (Scheme 1). This agrees with previous fs-studies of NR interacting with MOFs and other materials, where comparable time constants of hunreds of fs have been reported for the ICT event [19,20,27,28]. Figure S7 displays a comparison of the emission transients of NR when interacting with Zr-ITQ-HB and Al-ITQ-HB. The component of ICT in NR@Zr-ITQ-HB is slightly longer (~ 0.6 ps) than the one observed in NR@Al-ITQ-HB (~ 0.45 ps). The small difference might reflect the difference in the polarity of the environment of the surface (Zr vs Al clusters) in agreement with the steady-state emission behaviour of these composites. Finally, the ~ 10 ps component is assigned to the vibrational cooling (VC) of NR adsorbed in the MOF surface. This value is comparable to the one observed for the NR@Al-ITQ-HB (9 ps), and for NR when located within the Al-ITQ-HB framework [19]. However, this time is longer than those observed using other hosts, such as silica-based materials: MCM41 (3 ps) and zeolites (~ 1.5 ps). [27,28]. The difference could be explained in terms of a weaker NR@M – ITQ-HB complexes that are formed through nonspecific interactions, which is translated to a slower dissipation process of the excess energy (heat) to the MOFs when NR molecules are excited as considered here. Our explanation is supported by the fact that NR is quickly liberated in dichloromethane suspensions of NR@Zr-ITQ-HB and NR@Al-ITQ-HB, while NR@silica-based composites are robust [27,28].

3.5. Fluorescence lifetime imaging microscopy of NR@Zr-ITQ-HB

The NR@Zr-ITQ-HB composites were also studied by time-resolved fluorescence lifetime imaging microscopy (FLIM). Several single crystals were selected for analysis of their photobehaviours. No significant differences were found between the interrogated crystals, so Fig. 4 A and B shows representative decays and spectra in comparison with the ones obtained for the ensemble sample, respectively. The inset of Fig. 4B exhibits the image of the fluorescence lifetime distribution of a single crystal and at the bottom a picture of the solid. Table 4 gives the time constants and relative contributions (normalized to 100) ob-

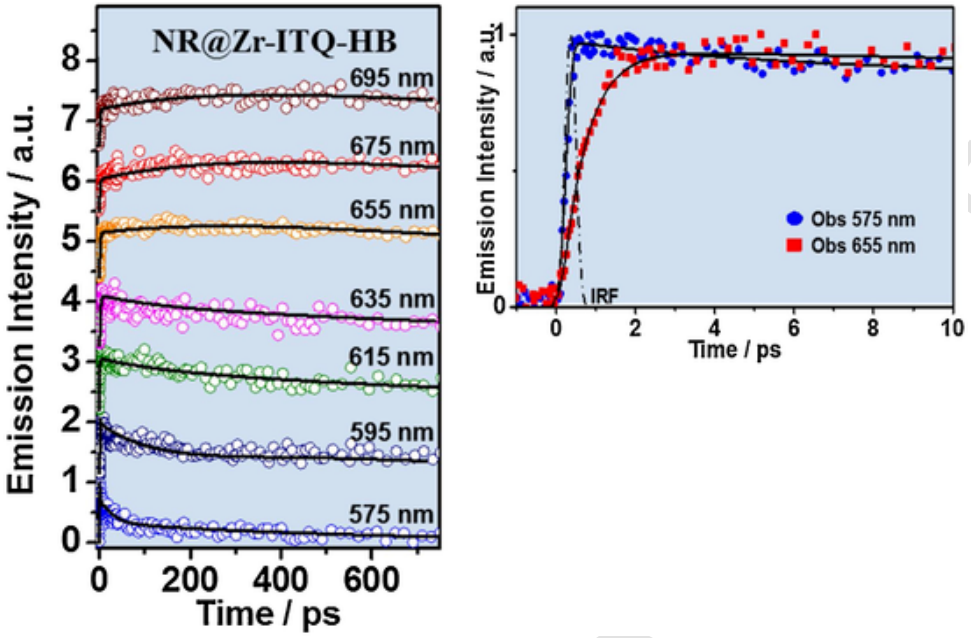

Fig. 3. (A) Femtosecond emission transients and (B) a zoom of the transients of NR@Zr-ITQ-HB in solid state upon excitation at 470 nm and observation at different wavelengths. The solid lines are from the best fits using a multiexponential function.

Table 3
Values of the time constants and normalized (to 100) pre-exponential factors (ai) obtained from a multiexponential fit of the femtosecond emission transients of NR@Zr-ITQ-HB upon excitation at 470 nm. The negative sing for a_i indicates a rising component in the emission signal.

$\lambda_{Obs/nm}$	τ_1/ps (±0.2)	a_1	τ_2/ps (±2)	a_2	τ_3/ps (±15)	a_3	τ_4/ps (±15)	a_4	τ_5/ns	a_5
575			10	37	150	25	299	38		
595			10	23	143	20	310	57		
615	0.65	-100	11	18	136	10	300	82		
635	0.61	-100			141	15	315	85		
655	0.59	-45					300	-55	1.18	100
675	-	-					325	-100		100
695	-	-					323	-100		100

tained from multiexponential fits of the emission decays of the single crystal collected at two representative spectral ranges (590 - 640 nm and 645 - 800 nm), as well as the values obtained for the ensemble solid in the ps experiments at the corresponding wavelengths. To make an accurate fit, we needed four components having time constants of 0.43, 0.91, 2.50 and 4.20 ns. The shortest one (0.43 ns), which decays at the greenest region and rises at the reddest one, is assigned to the ET process between the adsorbed neighbouring NR molecules, while the longest component (4.20 ns) is attributed to the emission of species having suffered an ET event. In comparison with the times observed for the ensemble solid (0.34 and 3.3 ns, respectively), the ones for the single crystals (0.43 and 4.20 ns, respectively) are slightly longer (Fig. 4A). We explain the decrease in the values for the ensemble solid in terms of quenching processes between neighbouring crystals. The two intermediate lifetimes, 0.9 and 2.5 ns, are attributed to the emission decays of aggregates and the charge separated (CS) state, respectively. Note that these components, considering their contributions in the signal, can be averaged and give 1.2 ns lifetime, a comparable value to the observed in the ensemble solid, and which we assigned to a combination of lifetimes of NR emitting from the CS state and of the aggregates. Under the microscope, we can interrogate single crystals and thus eliminate the inter-crystal interactions not avoidable in the ensemble sample, which allows us to distinguish better both species. Fig. 4 B shows a comparison of the emission spectra of the single crystals and the ensemble ones. The single crystals emission spectrum has its maximum of emission intensity at ~ 665 nm. This is about 20 nm blue shifted in comparison with the ensemble solid emission band. We explain this difference in terms of the interactions between the crystals in the ensemble solid samples, giving rise to the redder emission in the ensemble solid. Analysing several crystals and at different points within the same crystal gives comparable emission spectra, which indicates that the NR species are homogenously distributed along the framework, in agreement with the FLIM image of the single crystals (inset of Fig. 4B).

4. Comparison between All the ITQ MOFs

In this section, we compare and discuss the new obtained results analysed above and those already reported by this research group studying NR interacting with the different MOFs of the ITQ family: Al-ITQ-HB, Al-ITQ-EB, Al-ITQ-AB and Zr-ITQ-HB, where HB = heptylbenzoate, EB = ethylbenzoate and AB = aminobenzoate (Scheme 2) [19–21]. Table 5 displays the values of the time constants obtained for the related photoprocesses and the fluorescence lifetimes recorded for the four different composites.

To start with, in solution (dichloromethane, DCM) the photodynamics of NR is characterized by an ultrafast ICT/VC process (~ 1 ps)

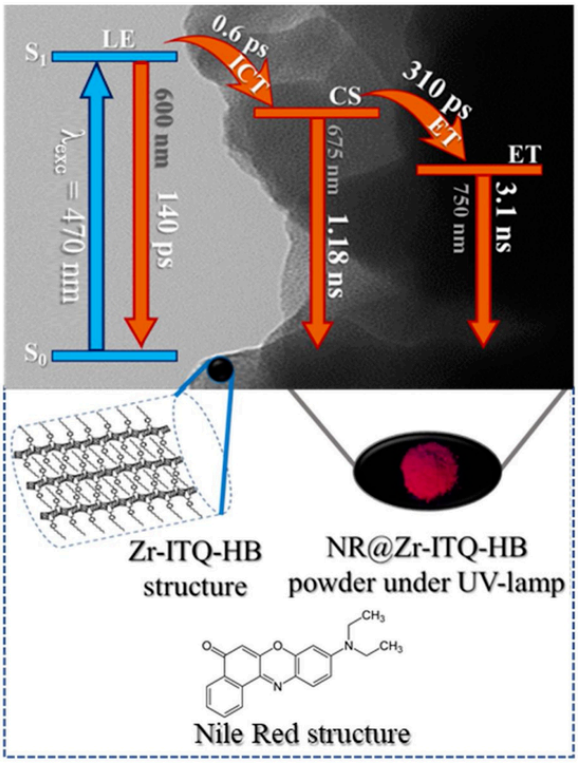

Scheme 1. Photodynamic schemes of NR@Zr-ITQ-HB composite. LE, ICT, CS and ET mean local excited state, intramolecular charge transfer, charge separated state and energy transfer, respectively. See text for more details. The under part reflects a scheme of the structure of the Zr-ITQ-HB, an image of the emission of the NR@Zr-ITQ-HB under the UV-lamp (360 nm) and the molecular structure of Nile Red.

and the emission from the CS state (~ 4.4 ns) [25]. The ultrafast ICT reaction of NR when interacting with the different MOFs is conditioned by the environment created by the inorganic part of the materials. When the presence of polar metal centres is higher (because the organic content is lower, as for Al-ITQ-EB and Al-ITQ-AB) the interaction between NR and the metal cluster stabilizes the excited NR molecules and this increases the barrier for the ICT, thus increasing the related time constant [20]. When the length of the alkyl chain of the linkers in the MOFs is comparable, but the metal cluster and the proportion with the organic linker are different (for example in NR@Al-ITQ-HB and NR@Zr-ITQ-HB composites), we observed that a larger fraction of organic content in Zr-MOF creates a less polar environment, slowing down the ICT reaction (0.6 vs 0.45 ps for Zr- and Al-ITQ-HB, respectively). Next, the VC process of the excited NR are not significantly affected by the nature of the material. The time for the process is ~ 10 ps in both NR@Al-ITQ-HB and NR@Zr-ITQ-HB. This process is much slower in comparison with the one for NR in DCM solution, where it occurs in ~ 1 ps (coupled with the ICT). This slowing down is explained in terms of less efficient heat dissipation in the composites due to weaker interaction of NR molecules with the surface of the studied MOFs. This explanation fits well with the fast liberation of NR molecules from these composites in a solvent suspension (about 1 ps), and contrary to what happens when NR is hosted by MCM41 and NaX/NaY zeolites [27,28]. In these later composites, the VC process of adsorbed NR is much faster: NR@MCM41 (3 ps) and NR@zeolites (~ 1.5 ps).

Interestingly, the distribution of the NR molecules on the surfaces of these 2D-MOFs favours the intermolecular interactions, leading to ET between neighbouring NR molecules. This photoinduced process is conditioned by the environment created by the organic linkers of the frameworks. The higher the organic linker proportion is, the slower the process becomes (Zr-ITQ-HB > Al-ITQ-HB > Al-IT Q-EB). Remarkably, for the amino derivative this reaction is completely inhibited by the transfer of an electron from the amino moiety of the linkers to the NR molecules [20]. The dependence of the ET on the dye concentration as observed in the NR@Al-ITQ-HB composites suggests that the process

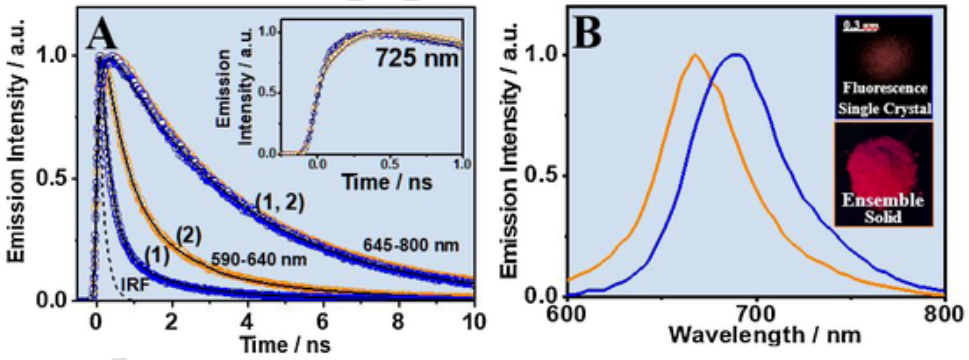

Fig. 4. (A) Comparison of the emission decays of NR@Zr-ITQ-HB recorded (1) under the fluorescence microscopy and (2) with the TCSPC technique. The insert shows an image of the emission of a single crystal and the ensemble solid under the UV-lamp (360 nm). The excitation wavelength was 470 nm and the decays were recorded at different observation wavelength regions as indicated in the figure. The solid line are from the best fit using a multiexponential function. (B) Emission spectra of NR@Zr-ITQ-HB of the (1) ensemble solid and of the (2) single crystal upon excitation at 470 nm.

Table 4
Comparison of the ensemble solid and the single crystals fluorescence emission lifetimes (τ_i) and normalized (to 100) pre-exponential factors (a_i) obtained from a multi-exponential fit of the emission decays of NR@Zr-ITQ-HB upon excitation at 470 nm.

$\lambda_{Obs/nm}$	τ_1/ns (±0.05)	a_1	τ_2/ns (±0.20)	a_2	τ_3/ns (±0.20)	a_3	τ_4/ns (±0.20)	a_4
550 - 650	0.43	30	0.91	43	2.50	18	4.20	8
650 - 800		-100		-		37		63

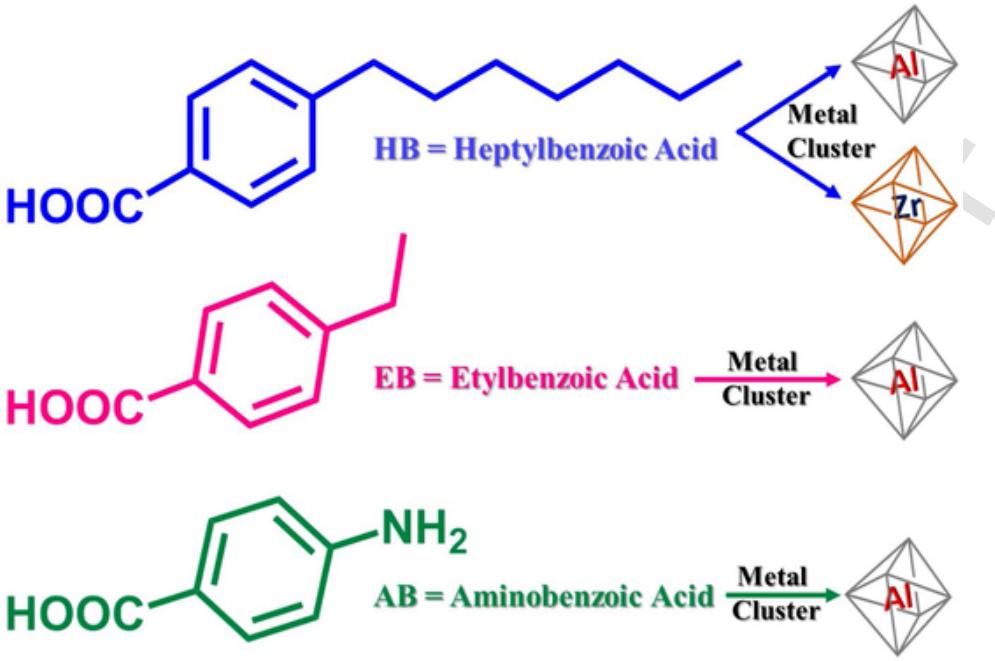

Scheme 2. Chemical structures of the organic linkers and metal clusters that compose the different studied MOFs.

Table 5
Comparison of the time values of the photoprocesses and the fluorescent lifetimes obtained for the composites NR@Al-ITQ-HB and NR@Zr-ITQ-HB.

	Photoprocesses				Fluorescence Lifetimes		
Composite	**ICT / ps**	**VC / ps**	**ET / ns**	**eT / ps**	**CSS / ns**	**ETS / ns**	**Aggregates / ns**
NR / DCM [(a)]	1.0	1.0	-	-	4.4	-	-
NR@Al-ITQ-HB [(b)]	0.42	9.0	0.22	-	0.22	3.61	1.33
NR@Al-ITQ-EB [(c)]	1.2	-	0.09	-	0.09	2.60	0.93
NR@Al-ITQ-AB [(c)]	1.0	-	-	17	0.13	-	0.54
NR@Zr-ITQ-HB	0.60	10.0	0.34	-	0.34	3.31	1.18

(a) From reference 25; (b) From reference 21; (c) From reference 20; ICT, VC, ET, eT, CSS and ETS means intramolecular charge transfer, vibrational cooling, energy transfer, electron transfer, electron injection, charge separated state and energy transfer state, respectively.

is mainly governed by Föster type of ET, although we cannot discard the presence of Dexter type ET due to the short distances between NR molecules distributed along the surfaces of the MOFs.

On the other hand, the length and nature of the linker chain in the MOF dictates the photoinduced processes of adsorbed NR molecules generating different emissive lifetimes. For example, a shortening in the alkyl chain (NR@Al-ITQ-EB) produces faster NR dynamics as the polarity of the medium is higher [20]. As a result, all the emissive species decay to the ground state in shorter times than in the NR@Al-ITQ-HB when the linker is longer having a 7 carbon atoms. When the alkyl chain of the MOF is replaced by an amino group (NR@Al-ITQ-AB), the photobehavior of the composite is remarkably different [20]. Femtosecond emission experiment shows a 17 ps component in the transients of NR@Al-ITQ-AB not present in the other composites. This very fast deactivation pathway is assigned to an electron transfer (eT) reaction from the amino phenyl group to the adsorbed NR molecules that efficiently deactivates the ET reaction [20]. Finally, the exchange of the Al-clusters by the Zr-ones affects the percent of the organic linkers. The dynamics of the former composites are slightly slower than the Al-based ones. In conclusion, we observe that the fluorescence lifetimes of the NR are clearly affected by both, the nature and length of the organic linker and of the metal clusters.

5. Conclusions

In this work, we reported on the effect of metal cluster of a 2D-MOF in the photobehavior of an organic dye supported on its surface. The change of the Al atoms by Zr ones in the ITQ-HB 2D-MOF generates a framework with a higher percent of the organic linker. This difference conditions the dynamics of the NR molecules located on the surfaces of the Zr-ITQ-HB. This MOF favours a distribution of the dye that results in ET reaction between neighbouring NR molecules. Nevertheless, the higher organic content of this material slows the ET, 0.34 ns, and the lifetime of the generated species, 3.6 ns. We also observed an ICT reaction in NR taking place in ~ 0.6 ps. This time component is also sensitive to the changes in the environment created by the MOF, as it increases in comparison with the one observed for the NR@Al-ITQ-HB. The ICT is followed by VC, which occurs in ~ 10 ps and is mostly independent of the metal cluster type or the organic linker content. Armed with FLIM technique, we studied the photobehaviour of single crystals, where the inter-crystal interactions are not present, and identified the emission decays associated with the aggregates (0.9 ns) and from the CS state (2.5 ns). Finally, we discuss how the nature of the metal cluster, the type of the organic linker and/or its relative content, affect the dynamics of the photoinduced processes in the adsorbed NR. Our findings may help in the design of new 2D-MOFs targeting the improvement of their applications in important fields of science and technology like photocatalysis and photonics.

Author contributions

The MOFs and their composites were made and characterized by the ITQ group. The spectroscopic experiments were designed, executed and analysed by the UCLM group. The manuscript was written through contributions of all authors. All authors have given approval to the final version of the manuscript.

Declaration of Competing Interest

The authors declare no conflict of interest.

Acknowledgments

This work was supported by MINECO through projects MAT2017-86532-R, and MAT2017- 82288-C2-1-P, and by the JCCM through project SBPLY/19/180501/000212. J.M.M. thanks the predoctoral fellowship from the Severo Ochoa program for support (SEV-2016-0683), and E.C.-M thanks the MINECO for the FPI fellowship (BES- 2015-071495).

Appendix A. Supplementary data

Supplementary material related to this article can be found, in the online version, at doi:https://doi.org/10.1016/j.jphotochem.2020.112887.

References

[1] J. Lee, O.K. Farha, J. Roberts, K.A. Scheidt, S.T. Nguyen, J.T. Hupp, Metal–organic framework materials as catalysts, Chem. Soc. Rev. 38 (2009) 1450–1459.
[2] H. Furukawa, K.E. Cordova, M. O'Keeffe, O.M. Yaghi, The chemistry and applications of metal-organic frameworks, Science 341 (2013).
[3] M.J. Kalmutzki, C.S. Diercks, O.M. Yaghi, Metal–Organic Frameworks for Water Harvesting from Air, Adv. Mater. 30 (2018).
[4] S. Yuan, L. Feng, K. Wang, J. Pang, M. Bosch, C. Lollar, Y. Sun, J. Qin, X. Yang, P. Zhang, Q. Wang, L. Zou, Y. Zhang, L. Zhang, Y. Fang, J. Li, H.-C. Zhou, Stable Metal–Organic Frameworks: Design, Synthesis, and Applications, Adv. Mater. 30 (2018) 1704303.
[5] A. Kirchon, L. Feng, H.F. Drake, E.A. Joseph, H.-C. Zhou, From fundamentals to applications: a toolbox for robust and multifunctional MOF materials, Chem. Soc. Rev. 47 (2018) 8611–8638.
[6] M. Bosch, M. Zhang, H.-C. Zhou, Increasing the Stability of Metal-Organic Frameworks, Adv. Chem. 2014 (2014).
[7] J. Ren, H.W. Langmi, B.C. North, M. Mathe, Review on processing of metal–organic framework (MOF) materials towards system integration for hydrogen storage, Int. J. Energy Res. 39 (2015) 607–620.
[8] S. Yuan, J.-S. Qin, C.T. Lollar, H.-C. Zhou, Stable Metal-Organic Frameworks with Group 4 Metals: Current Status and Trends, ACS Cent. Sci. 4 (2018) 440–450.
[9] C. Wang, X. Liu, N. Keser Demir, J.P. Chen, K. Li, Applications of water stable metal–organic frameworks, Chem. Soc. Rev. 45 (2016) 5107–5134.
[10] H. Furukawa, K.E. Cordova, M. O'Keeffe, O.M. Yaghi, The Chemistry and Applications of Metal-Organic Frameworks, Science 341 (2013) 1230444.
[11] T. Devic, C. Serre, High valence 3p and transition metal based MOFs, Chem. Soc. Rev. 43 (2014) 6097–6115.
[12] Y. Bai, Y. Dou, L.-H. Xie, W. Rutledge, J.-R. Li, H.-C. Zhou, Zr-based metal–organic frameworks: design, synthesis, structure, and applications, Chem. Soc. Rev. 45 (2016) 2327–2367.
[13] I. Abánades Lázaro, R.S. Forgan, Application of zirconium MOFs in drug delivery and biomedicine, Coord. Chem. Rev. 380 (2019) 230–259.
[14] B. Wang, X.-L. Lv, D. Feng, L.-H. Xie, J. Zhang, M. Li, Y. Xie, J.-R. Li, H.-C. Zhou, Highly Stable Zr(IV)-Based Metal–Organic Frameworks for the Detection and Removal of Antibiotics and Organic Explosives in Water, J. Am. Chem. Soc. 138 (2016) 6204–6216.
[15] A. Dhakshinamoorthy, A.M. Asiri, H. Garcia, 2D Metal–Organic Frameworks as Multifunctional Materials in Heterogeneous Catalysis and Electro/Photocatalysis, Adv. Mater. 31 (2019) 1900617.
[16] J.M. Moreno, A. Velty, J.A. Vidal-Moya, U. Díaz, A. Corma, Growth-modulating agents for the synthesis of Al-MOF-type materials based on assembled 1D structural subdomains, Dalton Trans. 47 (2018) 5492–5502.
[17] J.M. Moreno, A. Velty, U. Díaz, A. Corma, Synthesis of 2D and 3D MOFs with tuneable Lewis acidity from preformed 1D hybrid sub-domains, Chem. Sci. 10 (2018) 2053–2066.
[18] J.M. Moreno, A. Velty, U. Diaz, Expandable Layered Hybrid Materials Based on Individual 1D Metalorganic Nanoribbons, Materials (Basel, Switzerland) 12 (2019) 1953.
[19] E. Caballero-Mancebo, B. Cohen, J.M. Moreno, A. Corma, U. Díaz, A. Douhal, Exploring the Photodynamics of a New 2D-MOF Composite: Nile Red@Al–ITQ-HB, ACS Omega 3 (2018) 1600–1608.
[20] E. Caballero-Mancebo, J.M. Moreno, B. Cohen, U. Díaz, A. Corma, A. Douhal, Unravelling Competitive Electron and Energy-Transfer Events at the Interfaces of a 2D MOF and Nile Red Composites: Effect of the Length and Structure of the Linker, ACS Appl. Mater. Interfaces 10 (2018) 32885–32894.
[21] E. Caballero-Mancebo, J.M. Moreno, A. Corma, U. Díaz, B. Cohen, A. Douhal, How Does the Surface of Al–ITQ-HB 2D-MOF Condition the Intermolecular Interactions of an Adsorbed Organic Molecule?, ACS Appl. Mater. Interfaces 10 (2018) 20159–20169.
[22] P. García-García, J.M. Moreno, U. Díaz, M. Bruix, A. Corma, Organic-inorganic supramolecular solid catalyst boosts organic reactions in water, Nat. Commun. 7 (2016) 10835-10835.
[23] J.M. Moreno, Síntesis de materiales híbridos orgánicos-inorgánicos estructurados a partir de unidades unidimensionales, Estudio de sus propiedades y aplicaciones, Instituto de Tecnología Química (UPV-CSIC), Universidad Politécnica de Valencia, 2018.
[24] M. Gutiérrez, F. Sánchez, A. Douhal, Efficient multicolor and white light emission from Zr-based MOF composites: spectral and dynamic properties, J. Mater. Chem. C 3 (2015) 11300–11310.
[25] C. Martín, P. Piatkowski, B. Cohen, M. Gil, M.T. Navarro, A. Corma, A. Douhal, Ultrafast Dynamics of Nile Red Interacting with Metal Doped Mesoporous Materials, J. Phys. Chem. C 119 (2015) 13283–13296.
[26] M. Yoon, S.Y. Ryu, Characteristics of excited-state intermediates of TiO2–Y-Zeolite and MCM41 encapsulating photosensitive molecules: design of new photocatalysts, Res. Chem. Intermed. 30 (2004) 207–233.
[27] C. Martin, B. Cohen, M.T. Navarro, A. Corma, A. Douhal, Unraveling the ultrafast behavior of nile red interacting with aluminum and titanium co-doped MCM41 materials, Phys. Chem. Chem. Phys. 18 (2016) 2152–2163.
[28] M.R. di Nunzio, E. Caballero-Mancebo, C. Martín, B. Cohen, M.T. Navarro, A. Corma, A. Douhal, Femto-to nanosecond photodynamics of Nile Red in metal-ion exchanged faujasites, Microporous Mesoporous Mater. 256 (2018) 214–226.
[29] J. Organero, L. Tormo, A. Douhal, Caging ultrafast proton transfer and twisting motion of 1-hyroxyl-2-acetonapthone, Chem. Phys. Lett. 363 (2002) 409–414.
[30] Angiolini, L., B. Valetti S Fau - Cohen, A. Cohen B Fau - Feiler, A. Feiler A Fau - Douhal, A. Douhal, Fluorescence imaging of antibiotic clofazimine encapsulated within mesoporous silica particle carriers: relevance to drug delivery and the effect on its release kinetics,.
[31] B. Cohen, C. Martin, S.K. Iyer, U. Wiesner, A. Douhal, Single Dye Molecule Behavior in Fluorescent Core–Shell Silica Nanoparticles, Chem. Mater. 24 (2012) 361–372.